Tide-surge Interaction Intensified by the Taiwan Strait

Wen-Zhou Zhang,[1,2,3] Fengyan Shi,[3] Hua-Sheng Hong,[1] Shao-Ping Shang,[2] and James T. Kirby[3]

Received 27 August 2009; revised 4 January 2010; accepted 7 January 2010; published 19 June 2010.

[1] The Taiwan Strait is a long and wide shelf-channel where the hydrodynamics is extremely complex, being characterized by strong tides, and where storm surges frequently occur during the typhoon season. Obvious oscillations due to tide-surge interaction were observed by tide gauges along the northern Fujian coast, the west bank of the Taiwan Strait, during Typhoon Dan (1999). Numerical experiments indicate that nonlinear bottom friction (described by the quadratic formula) is a major factor to predict these oscillations while the nonlinear advective terms and the shallow water effect have little contribution. It is found that the tide-surge interaction in the northern portion of the Taiwan Strait is intensified by the strait. Simulations based on simplified topographies with and without the island of Taiwan show that, in the presence of the island, the channel effect strengthens tidal currents and tends to align the major axes of tidal ellipses along the channel direction. Storm-induced currents are also strengthened by the channel. The pattern of strong tidal currents and storm-induced currents along the channel direction enhances tide-surge interaction via the nonlinear bottom friction, resulting in the obvious oscillations along the northern Fujian coast.

Citation: Zhang, W.-Z., F. Shi, H.-S. Hong, S.-P. Shang, and J. T. Kirby (2010), Tide-surge Interaction Intensified by the Taiwan Strait, *J. Geophys. Res.*, *115*, C06012, doi:10.1029/2009JC005762.

1. Introduction

[2] The Taiwan Strait is located on the wide continental shelf of the China Seas, bounded by the island of Taiwan to the east and the Chinese mainland to the west. It is a long and wide channel connecting the East China Sea and the South China Sea. The average depth of the strait is nearly 60 m.

[3] Tidal range in the Taiwan Strait has a large spatial variation. The mean tidal range in its northwest end is larger than 4 m while that in the southeast end is smaller than 1 m. The remarkable spatial difference in tidal range results in extremely strong currents [*Fang et al.*, 1985]. The semidiurnal tide is dominant in the Taiwan Strait. Both observations and numerical model results have shown that the major axes of ellipses of M_2 and K_1 tidal constituents are in the direction along the strait [*Jan et al.*, 2002; *Lin et al.*, 2005].

[4] The Taiwan Strait is on the west edge of the western North Pacific (WNP) where tropical cyclones form frequently. Tropical cyclones formed in the WNP account for over 30% of events occurring worldwide [*Gray*, 1968; *Lander and Guard*, 1998]. There are about 6–8 typhoons, or strong tropical cyclones, affecting the strait every year. Typhoons often induce storm surge and coastal inundation, causing heavy damage to property and loss of life. Based on the data given by *Yang et al.* [1993], there were 69 typhoons inducing high storm surges over 1 m at the Fujian coast, the western bank of the Taiwan Strait, from 1949 to 1990, four of which caused a storm surge elevation over 2 m. Among them, Typhoon Elsie (1961) induced a fatal storm surge over 2 m and inundation at the northwest coastal area of the Taiwan Strait and 7770 people were killed. Since 1990, there were several strong typhoons affecting the Taiwan Strait and accompanying with them, devastating storm surges appeared along the Fujian coast. They destroyed coastal infrastructure and caused severe disasters. For example, Typhoon Dan (1999) caused a damage of four billion Chinese yuan and a loss of 72 people. Frequent occurrence and high risk attracted much attention to the storm surge and its prediction technique.

[5] Tide-surge interaction is one of the most important problems in the study and the prediction of storm surges [*Proudman*, 1955a; *Doodson*, 1956; *Wolf*, 1981; *Bernier and Thompson*, 2007]. In early pioneering work, *Proudman* [1955a, 1955b, 1957] conducted theoretical investigations on the effect of tide-surge interaction on storm surges in an estuary and showed that tide-surge interaction makes the height of a storm surge whose peak occurs near to tidal high water less than that of a surge whose peak occurs near to tidal

[1]State Key Laboratory of Marine Environmental Science, Xiamen University, Xiamen, China.
[2]Key Laboratory of Underwater Acoustic Communication and Marine Information Technology of the Minister of Education, Xiamen University, Xiamen, China.
[3]Center for Applied Coastal Research, Department of Civil and Environmental Engineering, University of Delaware, Newark, Delaware, USA.

0148-0227/10/2009JC005762

low water for a progressive wave, while the effect is reversed for a standing oscillation. *Doodson* [1956] studied the tide-surge interaction in a long uniform gulf and showed that the interaction between tide and surge affects the shapes and heights of the storm surges. According to studies since mid-1950s, tide-surge interaction cannot be neglected in predictions of storm surges in shallow water. The tide-surge interaction in the North Sea and River Thames was extensively investigated in several studies by *Rossiter* [1961], *Banks* [1974], *Prandle and Wolf* [1978], and *Wolf* [1981]. The main contributions of their work to the literature have been described amply in *Bernier and Thompson* [2007] and *Horsburgh and Wilson* [2007]. Recently, *Horsburgh and Wilson* [2007] confirmed the reported tendency for peak residuals to occur most frequently on the rising tide based on 1993–2005 data from the five sites on the east coast of the United Kingdom. Attention has been paid to the importance of tide-surge interaction in some other regions. *Johns et al.* [1985] showed that tide-surge interaction produces a substantial effect off the Orissa coast of India and causes the sea surface elevation either to increase above or to decrease below its pure surge value. *As-Salek and Yasuda* [2001] found that the tide-surge interaction in the Meghna estuary of Bangladesh displays the progressive wave nature of local tide. *Wang and Chai* [1989] indicated that the periodic residuals during storm periods at Wusong on the coast of the East China Sea are mainly caused by the interaction between tide and storm surge. *Bernier and Thompson* [2007] showed that the nonlinear parameterization of bottom stress is the principal contributor to their modeled tide-surge interaction off the east coast of Canada and northeastern United States.

[6] Although both large tidal ranges and frequent storm surges are observed in the Taiwan Strait, little attention has been paid to tide-surge interaction. Observations of storm surges often show oscillations with near-tidal period at the northern Fujian coast [*Wang and Liu*, 1986; *Zhang et al.*, 2004]. The purpose of this work was to investigate the oscillations due to tide-surge interaction and to explain the enhancing effect of the Taiwan Strait on the tide-surge interaction at the northern Fujian coast.

[7] The paper is organized as follows. The tide-surge model used in this work is briefly described in section 2. Section 3 describes the observations of oscillations with near-tidal period in the storm surge data during Typhoon Dan (1999) and the decisive factor of tide-surge interaction for the oscillations. In section 4, a series of numerical experiments is conducted to examine dynamic factors related to tide-surge interaction. Section 5 discusses the intensification caused by the Taiwan Strait on tide-surge interaction and its mechanism related to the nonlinear bottom friction. Results are summarized and concluded in section 6.

2. Tide-Surge Model

2.1. Numerical Model

[8] The numerical model (the two-way Nested Coupled Tide-Surge Model, NCTSM) is described in detail by *Zhang et al.* [2007] and is used to forecast typhoon surges by three operational forecast agencies (Oceanic and Fishery Bureau of Fujian Province, Fujian Marine Forecast Center, and Ningde Marine Forecast Center) in Fujian Province since 2007. It is a 2-D barotropic model based on depth-averaged momentum and continuity equations in the spherical coordinates as follows:

$$\frac{\partial u}{\partial t}+\frac{u}{R\cos\varphi}\frac{\partial u}{\partial \lambda}+\frac{v}{R}\frac{\partial u}{\partial \varphi}-\frac{uv\tan\varphi}{R}-fv = -\frac{g}{R\cos\varphi}\frac{\partial \zeta}{\partial \lambda}-\frac{1}{\rho R\cos\varphi}\frac{\partial p_a}{\partial \lambda}+\frac{1}{\rho H}(F_s-F_b) \quad (1)$$

$$\frac{\partial v}{\partial t}+\frac{u}{R\cos\varphi}\frac{\partial v}{\partial \lambda}+\frac{v}{R}\frac{\partial v}{\partial \varphi}+\frac{u^2\tan\varphi}{R}+fu = -\frac{g}{R}\frac{\partial \zeta}{\partial \varphi}-\frac{1}{\rho R}\frac{\partial p_a}{\partial \varphi}+\frac{1}{\rho H}(G_s-G_b) \quad (2)$$

$$\frac{\partial \zeta}{\partial t}+\frac{1}{R\cos\varphi}\left[\frac{\partial (Hu)}{\partial \lambda}+\frac{\partial (Hv\cos\varphi)}{\partial \varphi}\right]=0, \quad (3)$$

where the notations are the same as those given by *Zhang et al.* [2007]. t represents the time; (λ,φ) represent the east longitude and north latitude; (u,v) represent the east and north components of the depth-averaged velocity $\mathbf{q}$; ζ represents the sea surface elevation above the undisturbed sea level; H represents the total water depth, $H = h + \zeta$; h represents the depth of undisturbed water; p_a represents the atmospheric pressure on the sea surface; $\boldsymbol{\tau}_b = (F_b, G_b)$ represents the bottom friction; and $\boldsymbol{\tau}_s = (F_s, G_s)$ represents the wind stress. Two-dimensional models are widely adopted in the studies on tide-surge interaction and in the operational forecast of storm surge [e.g., *Banks*, 1974; *Wolf*, 1981; *Tang et al.*, 1996; *Flather*, 2000; *As-Salek and Yasuda*, 2001; *Shen et al.*, 2006; *Bernier and Thompson*, 2007; *Horsburgh and Wilson*, 2007]. Although recent results [*Weisberg and Zheng*, 2008] indicate that 3-D models can give significantly different results for predicted surges owing to differences in the orientation and magnitude of the bottom stress vector, the 2-D model is applied in this work.

[9] For analysis of tide-surge interaction, ζ is usually considered to be the algebraic sum of tide level (ζ_T), pure storm surge elevation (ζ_S, sea level change produced by atmospheric forcing only), and residual elevation due to tide-surge interaction (ζ_I) [*Banks*, 1974], namely, $\zeta = \zeta_T + \zeta_S + \zeta_I$. Practical storm surge (ζ_{SI}) is the sum of the latter two parts ($\zeta_{SI} = \zeta_S + \zeta_I = \zeta - \zeta_T$). ζ, ζ_T, and ζ_S can be obtained by three control model runs, respectively, one with full forcing including atmospheric forcing and tidal forcing (full run), one with tidal forcing only (tide-only run), and one with atmospheric forcing only (storm-only run). Then, ζ_{SI} and ζ_I can be calculated from the results of above three model runs: $\zeta_{SI} = \zeta - \zeta_T$ and $\zeta_I = \zeta_{SI} - \zeta_S$. Since ζ_I is the result of tide-surge interaction, it can be taken as a direct measure of the interaction [*Bernier and Thompson*, 2007]. The root-mean-square (RMS) value of ζ_I can be used to determine the magnitude or the intensity of the oscillations due to tide-surge interaction during an entire storm event [*Bernier and Thompson*, 2007]. The ratio (referred to as I_r) of RMS(ζ_I) to RMS(ζ_S) can reflect total relative intensity of tide-surge interaction and pure storm surge.

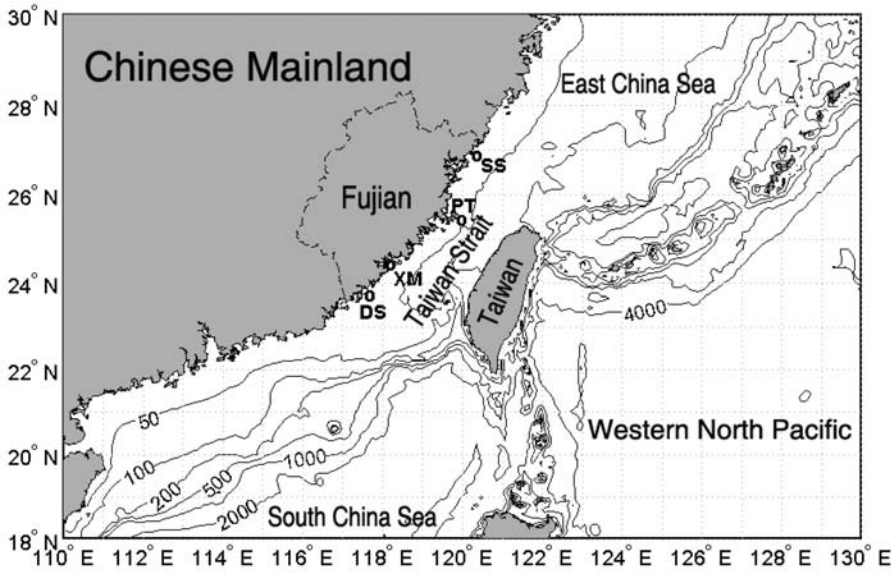

Figure 1. The geographic map and model domain. Water depth contours are in meters. SS: Sansha; PT: Pingtan; XM: Xiamen; DS: Dongshan.

[10] The quadratic law is applied in the parameterization of bottom stress ($\boldsymbol{\tau}_b$) and wind stress ($\boldsymbol{\tau}_s$) as follows:

$$\boldsymbol{\tau}_b = \rho C_b |\mathbf{q}|\mathbf{q}, \tag{4}$$

$$\boldsymbol{\tau}_s = \rho_a C_d |\mathbf{W}|\mathbf{W} \tag{5}$$

where C_b is the bottom friction coefficient which can be a constant or calculated using Chezy formula, i.e., $C_b = gc^{-2}$, $c = H^{1/6}/n$ in which n is Manning coefficient. Chezy formula with $n = 0.0295$ was used in this study. $\mathbf{W}$ is the wind velocity vector at a height of 10 m above sea surface; ρ_a is the density of air; and C_d is the wind stress coefficient and

$$C_d \times 10^3 = \begin{cases} 1.052, & |\mathbf{W}| \le 6\ \mathrm{m\,s^{-1}} \\ 0.638 + 0.069|\mathbf{W}|, & 6 < |\mathbf{W}| < 30\ \mathrm{m\,s^{-1}} \\ 2.708, & |\mathbf{W}| \ge 30\ \mathrm{m\,s^{-1}} \end{cases}, \tag{6}$$

which has been used by *Zhang et al.* [2007] and *Zhang et al.* [2009].

[11] The model domain is shown in Figure 1. The horizontal resolution is 1/10° (about 11.1 km) both in latitude and in longitude for the coarse structured mesh (110°E~130°E, 18°N~30°N) and 1/30° (about 3.7 km) for the fine mesh (113.3°E~121.5°E, 22.0°N~28.4°N). The coarse mesh mantles the whole fine mesh. Only the coarse mesh was used in this study to keep domain boundaries consistent in all numerical experiments. No water is allowed to flow through the coastal boundaries by making the normal component of current vanish. On the open boundaries, a radiation condition is used as follows [*Zhang et al.*, 2007; *Zhang et al.*, 2009]:

$$q_n = \hat{q}_n \pm \frac{C}{H}\left(\zeta - \hat{\zeta}\right), \quad C = \sqrt{gH} \tag{7}$$

where the subscript n stands for the component normal to the open boundary; $\hat{\zeta}$ is the water level input on the open boundary which is prescribed beforehand; and $\hat{q}_n$ is the current input determined by local solution. More details about the NCTSM are given by *Zhang et al.* [2007].

2.2. Tropical Cyclone Model

[12] A tropical cyclone (typhoon or hurricane) is a strong tropical weather system with cyclonic wind field and low central air pressure. In this work, an analytic axisymmetric model, which is presented by *Holland* [1980] and is widely used in the operational forecasting of storm surges produced by a tropical cyclone, is applied to describe the wind field and air pressure field associated with a static cyclone. *Holland* [1980] demonstrated that this model is better than the modified Rankine vortex since the latter is too sensitive to the estimation of the radius to maximum wind. It includes two equations of the radial profiles of sea level pressure and winds in a cyclone and makes the air in cyclostrophic balance. The air pressure profile is given by the following equation:

$$p_a = p_c + \Delta p \exp\left[-\left(\frac{r}{r_m}\right)^{-B}\right], \ \Delta p = p_e - p_c, \ \ r > 0, \tag{8}$$

where p_c (Pa) is the central pressure of the cyclone, p_e (Pa) the ambient pressure or environmental pressure, and Δp the pressure drop or the pressure deficit; B is the shape parameter; r is the distance from the center, and r_m is the radius to maximum wind speed W_m. The wind profile is as follows:

$$W_c = W_m\left[\gamma^B \exp\left(1 - \gamma^B\right)\right]^{1/2}, \ \gamma = \frac{r_m}{r}. \tag{9}$$

where W_c is the wind speed at the distance r from the center. In equations (8) and (9), the shape parameter B can be calculated by the following formula developed from the studies

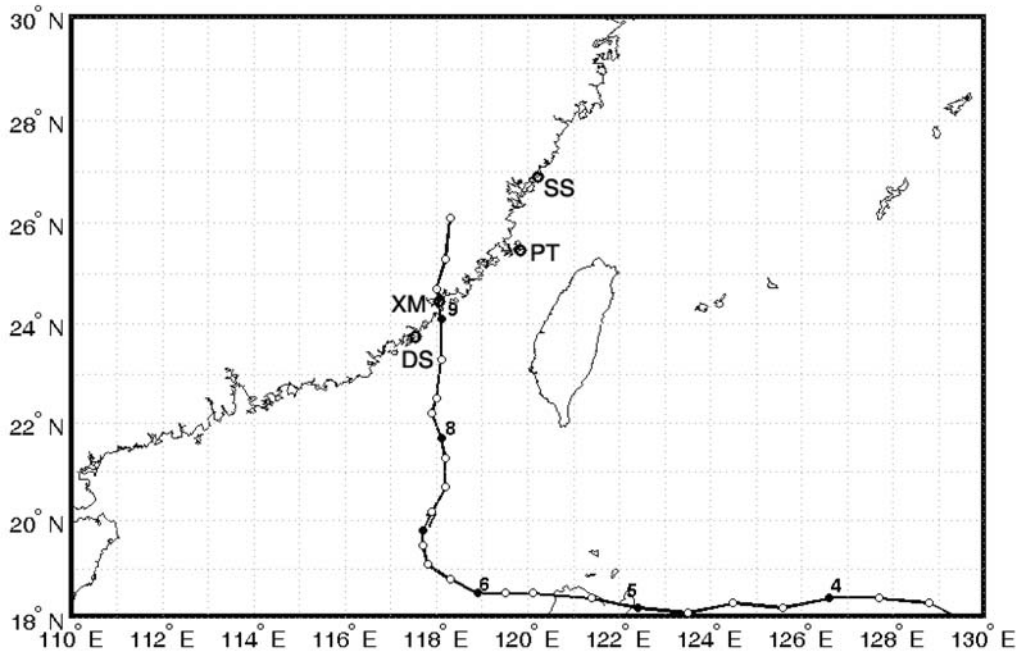

Figure 2. The best track of Typhoon Dan (1999) during the period from 3–10 October. Black dots denote the positions of the typhoon at 0800 local standard time (LST) on the dates labeled by numbers; circles denote the positions at 0200, 1400, or 2000 LST.

of *Atkinson and Holliday* [1977], *Jakobsen and Madsen* [2004], and *Zhang et al.* [2007]:

$$B = \alpha(P_e - P_c)^{\beta} + \varepsilon, \tag{10}$$

where α, β, and ε are empirical coefficients and are given by 0.095, 0.288, and 0.1, respectively, in this study.

[13] Since the wind field of a tropical cyclone circumrotates around its center, the wind direction is ideally tangent to the concentric circles. Because of friction effects, the actual wind direction deflects to the center an angle (inflow angle) from the tangential direction.

[14] The above wind profile is for the static cyclone. An additional wind field due to the motion of the cyclone [*Jelesnianski*, 1965] is added to the above static cyclone model. This tropical cyclone model is used in *Zhang et al.* [2009].

3. Oscillation due to Tide-Surge Interaction

3.1. Observations

[15] Typhoon Dan formed in the WNP on 4 October 1999. It moved west to the northeast area of the South China Sea, then turned north late on 6 October, and finally made landfall near Xiamen. Its moving path is plotted in Figure 2 based on the path data published by the China Meteorological Administration.

[16] Typhoon Dan is a good case to study the oscillations due to tide-surge interaction at the northern Fujian coast. One reason is that tide gauges at Sansha and Pingtan at the northern coast of Fujian recorded significant residual signals which were not submerged in storm surge peaks since the gauges were far from the storm path. The other reason is that the wind field was scarcely affected by the high terrain of the island of Taiwan since the storm center stayed more than 200 km away from the island, and its 7 Beaufort scale radius was too small to reach the island. Previous studies showed that the high terrain of the island has a significant influence on the low wind field and pressure field of a typhoon passing by it [*Chang et al.*, 1993], which results in some unexpected variations in storm surges and contaminates the oscillations with near-tidal period. In this case, the uncertainty of atmospheric forcing due to the terrain of the island was avoided to the utmost because of the unique storm path.

[17] The water level observations used in this study were obtained with float-type tide gauges at four tide gauge stations along Fujian coast (Figure 1), managed by the State Oceanic Administration of China. Time series of measured storm surge at Sansha, Pingtan, Xiamen, and Dongshan are calculated by subtracting predicted astronomical tide with 170 tidal constituents from the observed water level data and are shown by black solid lines in Figure 3. Dashed and dotted lines in Figure 3 represent numerical results and will be described in section 3.2. The measured data show that the peak of surge reached 121 cm at Xiamen where Dan passed. Surges at Sansha and Pingtan stations were small but indicated obvious oscillations with the semidiurnal tidal period.

3.2. Simulations

[18] Typhoon Dan was simulated using the NCTSM model described in section 2. To quantify the effect of tide-surge interaction, we carried out three runs: tide-only run, storm-only run, and full run. Eight tidal constituents, including M_2, S_2, N_2, K_2, K_1, O_1, P_1, and Q_1, were taken into account in tide simulations. The three runs were fully spun-up prior to extracting results in the storm period. We used pure storm surge ζ_S, practical storm surge ζ_{SI}, and residual ζ_I to represent,

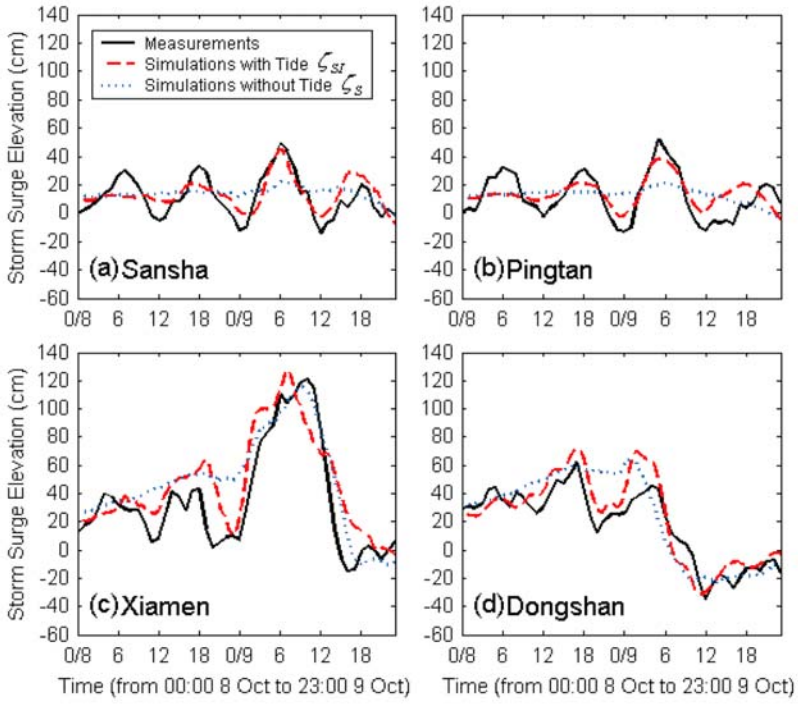

Figure 3. Time series of measured and predicted storm surges during the period from 0000 LST 8 October to 2300 LST 9 October 1999.

respectively, predicted surge without tide-surge interaction, surge with tide-surge interaction, and residual due to tide-surge interaction. They were obtained using the algebra defined in section 2.1.

[19] Figure 3 shows the time series of measured storm surge, model-predicted pure storm surge, and practical storm surge, respectively, at Sansha, Pingtan, Xiamen, and Dongshan. The full run predicted the oscillation patterns which match the measured surges in both magnitude and phase. Especially at Sansha and Pingtan, located at the northern Fujian coast, the magnitudes of the oscillations are more than 40 cm in both the measured data and the full run results, while the pure surges calculated from the storm-only run are less than 27 cm at the two gauges. The values of I_r are 0.649, 0.557, 0.244, and 0.334 at Sansha, Pingtan, Xiamen, and Dongshan, respectively, indicating that the tidal modulation at former two stations is more important than at the latter two. The intensity of tide-surge interaction is demonstrated by plots of residual shown in Figure 4. The magnitudes of the residuals are slightly larger than the storm-only induced surges, suggesting that tide-surge interaction is important in this region.

[20] It was noted that although wetting and drying schemes were not considered in the model [*Zhang et al.*, 2007], both tide simulations (refer to *Zhang et al.* [2007]) and storm surge simulations during Typhoon Dan were still in good agreement with measurements, indicating that the inundation process had little impact on tide-surge interaction in this area and the model was appropriate to this study.

4. Dynamic Factors for the Oscillation

[21] In studies of tide-surge interaction, mechanisms of the interaction are usually examined using a numerical modeling technique which separates the contribution to the interaction

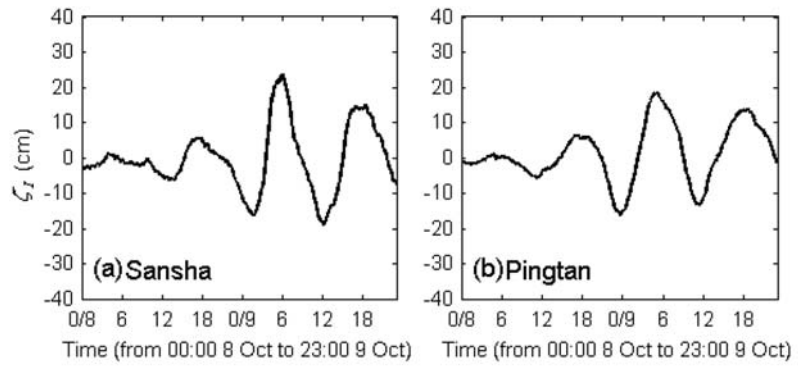

Figure 4. Time series of simulated residuals due to tide-surge interaction.

[e.g., *Prandle and Wolf*, 1978; *Bernier and Thompson*, 2007]. Tide-surge interaction is a nonlinear phenomenon and is mathematically attributed to nonlinear terms in the equations of motion. The governing equations (1) to (3) contain several nonlinear terms which can be classified into three nonlinear effects: (a) advective effect arising from the advective terms as shown in the momentum equations (1) and (2); (b) nonlinear effect of bottom friction terms with quadratic parameterization in (4); and (c) shallow water effect which arises from nonlinear terms related to $(h + \zeta)$ in mass conservation equation (3) and in momentum equations (1) and (2). The terminology "shallow water effect" was used by many authors who did not refer to the same terms in the nonlinear shallow water equations [e.g., *Proudman*, 1955a; *Prandle and Wolf*, 1978; *Horsburgh and Wilson*, 2007]. Here, in this paper, we refer shallow water effect to the effect from the terms related to $(h + \zeta)$. Details will be described in section 4.3.

[22] Previous studies showed that the significance of three effects may be case dependent and more related to specific regions associated with topography, tidal range, and strength of storm [*Proudman*, 1957; *Prandle and Wolf*, 1978; *Bernier and Thompson*, 2007; *Horsburgh and Wilson*, 2007]. To examine the three nonlinear effects in prediction of residuals in the Taiwan Strait, we carried out numerical experiments using reduced models by eliminating or linearizing nonlinear terms associated with each nonlinear effect. The results calculated from the model including all three effects (standard model/case) will be used as a reference, namely, standard results (see section 3.2), for comparisons with results from the reduced models.

4.1. Nonlinear Advective Effect

[23] After removing advective terms in momentum equations, we followed the same procedures as in the standard case and performed three model runs, i.e., tide-only run, storm-only run, and full run. Surges with and without tide-surge interaction (ζ_{SI} and ζ_S) and residuals (ζ_I) were obtained in the same way as in the standard case. Comparisons of residuals between the standard case and the case without advective terms (the figure omitted) show that the results of the two cases are very close, indicating that removing advective terms has little effect. Since the RMS value of residual ζ_I is used to quantify the intensity of tide-surge interaction, the reduction ratio of RMS(ζ_I) between the reduced model and the standard model can be calculated via the following formula:

$$I_p = \frac{RMS(\zeta_{ISC}) - RMS(\zeta_I)}{RMS(\zeta_{ISC})} \times 100\% \qquad (11)$$

where I_p represents the reduction ratio and ζ_{ISC} and ζ_I are residuals from the standard model and the reduced model, respectively. The reduction ratios are 4.7% at Sansha and 6.2% at Pingtan calculated from the hourly data during the storm period from 00:00 local standard time (LST) 8 October to 23:00 LST 9 October 1999. Based on the scaling analysis of momentum equations controlling tide and storm surge motions, the nonlinear advective term is an order of magnitude smaller than the quadratic bottom friction term (discussed in the following section) in the Taiwan Strait, indicating that the advective effect is insignificant for the tide-surge interaction in this area, compared with the bottom friction effect.

4.2. Nonlinear Bottom Friction

[24] To examine the influence of nonlinear bottom friction on tide-surge interaction, we set up a reduced model in which the quadratic form of bottom friction was replaced with a linear form,

$$\boldsymbol{\tau}_b = \rho C_{bl} \mathbf{q}, \qquad (12)$$

where C_{bl} is the coefficient of the linear bottom friction. The value of C_{bl} in the linear form of bottom friction may be inconsistent with that of C_b in the quadratic form. *Heaps* [1969] used a value $C_{bl} = 0.0024$ m s^{-1} in the linear bottom friction formulation for the North Sea. Here, we used a value $C_{bl} = 0.0020$ m s^{-1} which produced surges with peaks at Sansha and Pingtan comparable to those predicted by the nonlinear friction model.

[25] Three runs were conducted as in section 4.1. The same comparisons were made at Sansha and Pingtan as shown in Figure 5. Figures 5a and 5b show the time series of storm surges predicted by the reduced model with and without tide-surge interaction, with comparison to the measured data. The two results are almost identical and both of them disagree with measured data. Tidal modulations as shown in both measured data and the standard results were not predicted by the reduced model with linear bottom friction. Figures 5c and 5d show comparisons of residuals between the standard case and the case with linear bottom friction. The residuals predicted by the reduced model were very small, compared with the standard results. The discrepancy resulting from the linear bottom friction indicated that the nonlinear form of bottom friction is important in predicting tide-surge interaction. The reduction ratios I_p between the current case and the standard case are 83.6% at Sansha and 77.4% at Pingtan during the storm period. The high reduction ratios also implied that the nonlinear bottom friction is a major contributor to prediction of tide-surge interaction, which is consistent with the results in some other regions [e.g., *Tang et al.*, 1996; *Bernier and Thompson*, 2007].

[26] One concern about the residual oscillations almost disappearing in the reduced model is that the linear parameterization of friction is allowing much larger currents so that the surface stresses become negligible. From the comparison between the linear bottom friction and the quadratic bottom friction, the difference in using the different formulas can be measured by $C_r = C_b|\mathbf{q}|/C_{bl}$ with $C_r \sim 1$ representing that the same magnitude of bottom stresses can be obtained by both formulas. For general parameters in tide and storm surge simulations in the Taiwan Strait domain, the average depth of 60 m and current of ~ 1 m s^{-1} result in $C_r \sim 1$, indicating that the linear bottom friction formula may produce bottom stresses comparable to those from the quadratic formula. Figure 6 shows the comparisons of simulated currents and bottom stresses between the reduced model and the standard model. Surface stresses are also plotted in the figure for comparison. It can be seen from panels (a) and (b) that the currents simulated with linear bottom friction are comparable to those with quadratic one. Figure 6d shows that the nonlinear and linear bottom stresses calculated at Pingtan have similar amplitudes as in the comparison of currents shown in Figure 6b. However, the nonlinear bottom stress calculated at Sansha is obviously smaller than the linear one as shown in Figure 6c although the currents separately simulated with

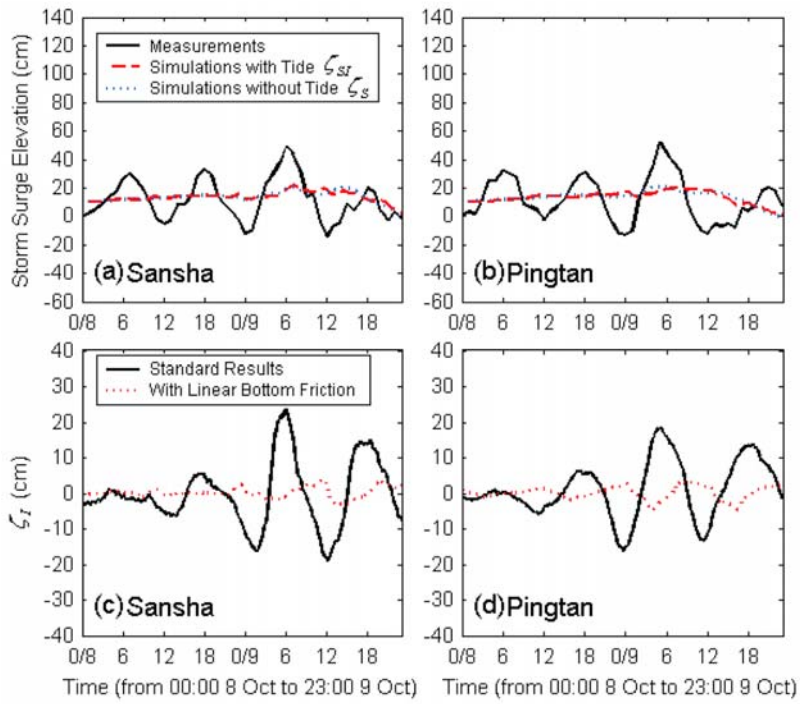

Figure 5. Time series of storm surges, (a and b) measured and simulated with a linear bottom friction form and (c and d) simulated residuals due to tide-surge interaction.

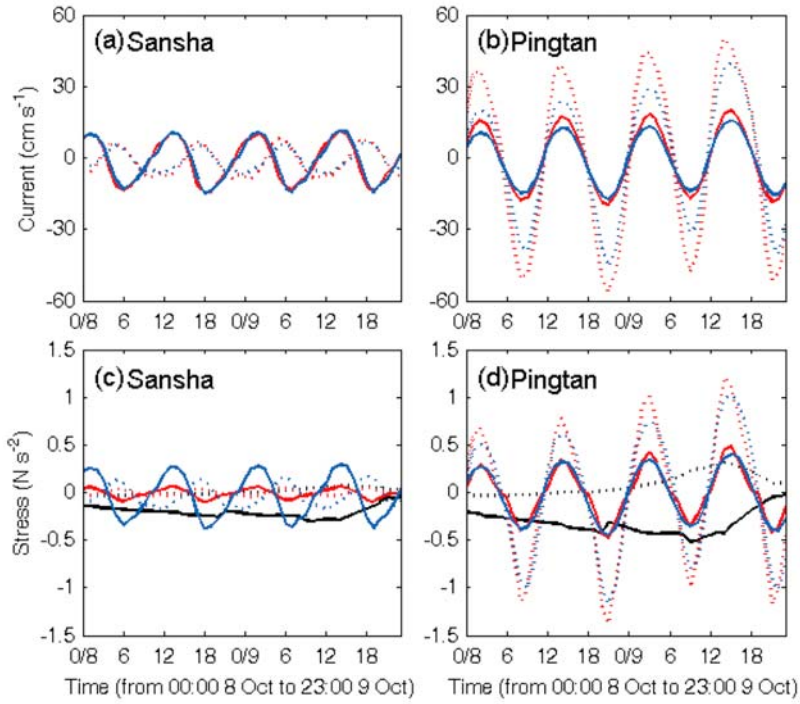

Figure 6. Time series of (a and b) current and (c and d) wind stress and bottom stress. Solid lines denote east components and dotted ones denote north components. Red solid and dotted lines are results (current and bottom stress) with nonlinear bottom friction; blue ones are results with linear bottom friction; black ones are wind stresses.

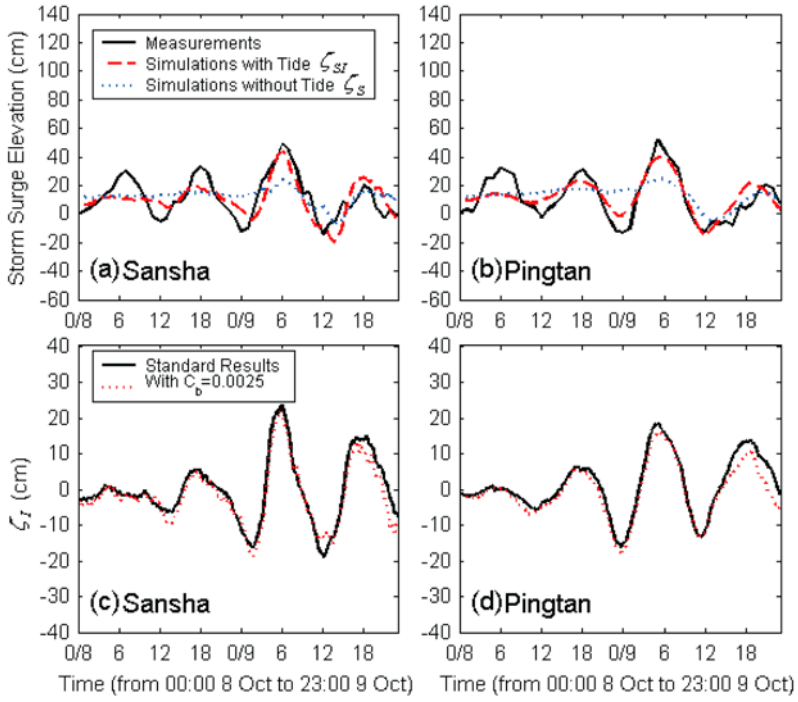

Figure 7. Time series of storm surges, (a and b) measured and simulated with a constant coefficient quadratic bottom friction form and (c and d) simulated residuals due to tide-surge interaction.

nonlinear and linear bottom friction formulas are almost the same in Figure 6a. These could be expected because, for the two specific stations, C_r is about 1 (H~10 m, $|\mathbf{q}| \sim 0.5$ m s^{-1}) at Pingran while C_r is quite smaller than 1 (H~10 m, $|\mathbf{q}| \sim$ 0.2 m s^{-1}) at Sansha. It is clear that the surface stress is not negligible in these two cases (Figures 6c and 6d), indicating that the wind stress is not swamped by the bottom stress.

[27] Another concern is that the coefficient of the nonlinear friction from equation (4) with the Chezy formula is dependent on the total water depth ($H = h + \zeta$) which should represent a nonlinear effect. In order to examine its influence on tide-surge interaction, we used a constant friction coefficient $C_b = 0.0025$ and repeated all simulations. Figures 7a and 7b show results from the model with constant friction coefficient, which are in good agreement with the measurements at Sansha and Pingtan like standard results. The comparisons of residuals in Figures 7c and 7d demonstrate that the differences caused by the two different types of coefficients are small. Thus, the oscillations due to tide-surge interaction were basically induced by the quadratic form of bottom friction rather than the depth-dependent coefficient.

4.3. Shallow Water Effect

[28] The effect of shallow water terms was initially named by *Proudman* [1957], who called the product term of surface elevation ζ and velocity u in the mass conservation equation and the advective term in the momentum equation the "shallow water terms." Later, *Prandle and Wolf* [1978] referred to the nonlinear terms containing $(h + \zeta)$ as shallow water terms. In this paper, we investigated the shallow water effects from the product terms in the mass conservation equation (3) and the terms which contain $(h + \zeta)$ in the denominator, in the momentum equations (1) and (2).

[29] We set up a reduced model by replacing occurrences of H ($= h + \zeta$) with h in the governing equations. Following the same procedures as in sections 4.1 and 4.2, we obtained surges with and without tide-surge interaction. Results of these simulations (not shown here) indicated that replacing H with h has little effect. The reduction ratios calculated were less than 20% at both Sansha and Pingtan, which was expected considering the small ratio of surface elevation to water depth. According to the result presented by *Wolf* [1981] and cited by *Horsburgh and Wilson* [2007], the shallow water effect may become dominant over quadratic friction only for tidal amplitudes in excess of 3 m and water depths of 10 m or less. In the Taiwan Strait, both the tidal amplitudes and surges in this case are less than 3 m [*Zhang et al.*, 2007], and the depths in most area are more than 10 m. Since the amplitudes of tides and surges are usually significantly smaller than water depths in the strait, water level variation contributes little to total water depth. In other words, the shallow water effect is not important in the strait. The results from the previous section and this section demonstrate that tidal modulation of storm surges arise dominantly through tidal current changes rather than tidal level variations in the northern part of the Taiwan Strait during Typhoon Dan.

5. Intensification of the Tide-Surge Interaction

[30] Based on scaling analysis [*Welander*, 1961; *Feng*, 1977], the significance of nonlinear effects can be measured by the ratio of surface elevation to water depth, e.g., $\kappa = \zeta/h$. Tide-surge interaction was believed to be a higher-order effect in estuaries or open coastal oceans [*Proudman*, 1957; *Liu and Wang*, 1989] if $\kappa \ll 1$ is satisfied. Residuals due to the nonlinear tide-surge interaction should be smaller in

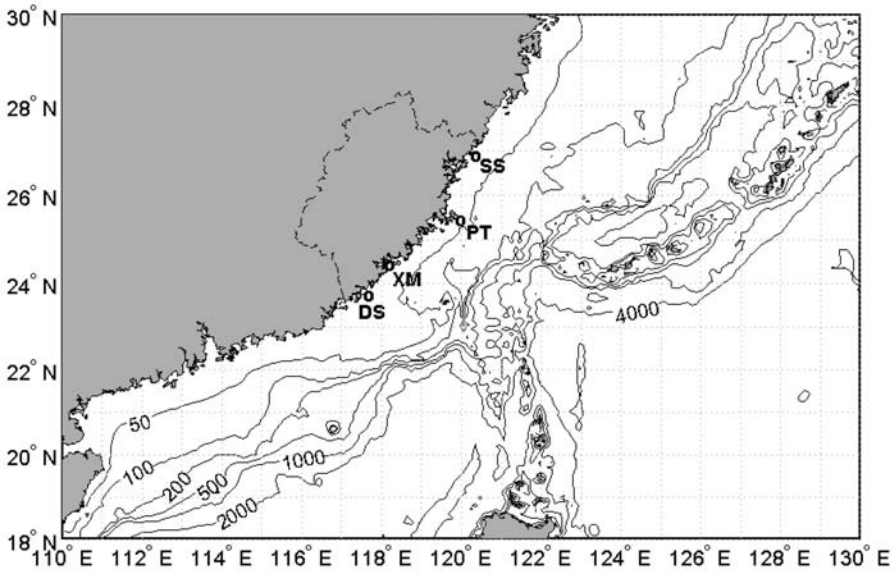

Figure 8. The bathymetry with the island of Taiwan replaced by artificial shelf bathymetry. Water depth contours are in meters.

magnitude than pure surges based on the weakly nonlinear assumption. However, in this study, numerical results at Sansha and Pingtan showed that the magnitude of oscillations caused by tide-surge interaction were even larger than pure surges driven by atmospheric forcing. That motivated us to investigate causes beyond the standard analysis. Our hypothesis was that the unique geological features of the Taiwan Strait may play an important role in tide-surge interaction.

[31] In this section, we conducted two sets of numerical experiments: one is with the real bathymetry but with the island of Taiwan removed from the computation domain; the other is with idealized coast and bathymetry with and without an island. The first experiment was used to reveal the role of the Taiwan Strait in tide-surge interaction. The second experiment was to examine hydrodynamic response to large-scale geological features without influences from small local bathymetric characteristics.

5.1. Experiment Without the Island

[32] The island of Taiwan was replaced by an artificial shelf region the bathymetry of which was obtained by linear interpolation using water depths around the island. Figure 8 shows the constructed bathymetry without the island.

[33] Simulations were carried out in the domain without the island following the same procedures and applying the same dynamic forcing (tidal forcing and atmospheric forcing) as in the standard case. Figures 9a and 9b show results from the simulations compared with measurements at Sansha and Pingtan. Although oscillations in the predicted practical surges ζ_{SI} are recognized, the magnitude of the oscillations is much smaller in this case than in the standard case (Figure 3). Figures 9c and 9d show comparisons of residuals due to tide-surge interaction ζ_I between the standard case and the case without island. The intensities of the oscillations measured by $1 - I_p$ are reduced to 44.9% and 53.9% at Sansha and Pingtan, respectively, relative to the standard case, suggesting that the island has a significant influence on tide-surge interaction in the Taiwan Strait.

5.2. Experiments With Idealized Coast and Bathymetry

[34] Although the above test case indicated that the island of Taiwan plays an important role in intensifying tide-surge interaction in the Taiwan Strait, some uncertainties in constructing the bathymetry without the island and the influence of small-scale geological features on tide-surge interaction are concerns. In order to confirm if the intensification of tide-surge interaction is mainly caused by the large-scale geological feature of the Taiwan Strait, we constructed an idealized topography including a curved coast line, an island, and shelf bathymetry according to basic geometric characteristics of the Taiwan Strait as shown in Figure 10a. The simplified coastline follows the sketch of the mainland coast. The island of Taiwan was simplified as a rectangle with size comparable to the island. The bathymetry contours follow the curve of the coastline, with water depth increasing linearly from 5 m at the coastline to 115 m at a distance comparable to the width of the Taiwan Strait, resulting in an average depth of about 60 m (the average depth in the Taiwan Strait). The rest of the seaward bathymetry was constructed using two slopes, one from 115 m to 200 m with a mild slope and the other from 200 m to 4000 m with a steep slope, and a submarine plain with a constant depth of 4000 m, as shown in Figures 10b and 11.

[35] Two idealized cases, one with the island (case 1 as shown in Figure 10b) and the other without island (case 2, Figure 10c), were examined with the same tidal forcing and atmospheric forcing as in the standard case. For comparisons between the standard case and the idealized cases, the model output was made at Point A and B marked in Figures 10b and 10c, corresponding to Pingtan and Sansha (also called Pingtan and Sansha for idealized cases).

5.2.1. Idealized Case With Island

[36] With the tidal boundary conditions as the same as in the standard case, the idealized model with island predicted tidal elevations comparable to the standard case at Sansha and Pingtan as shown in Figures 12a and 12b. The idealized

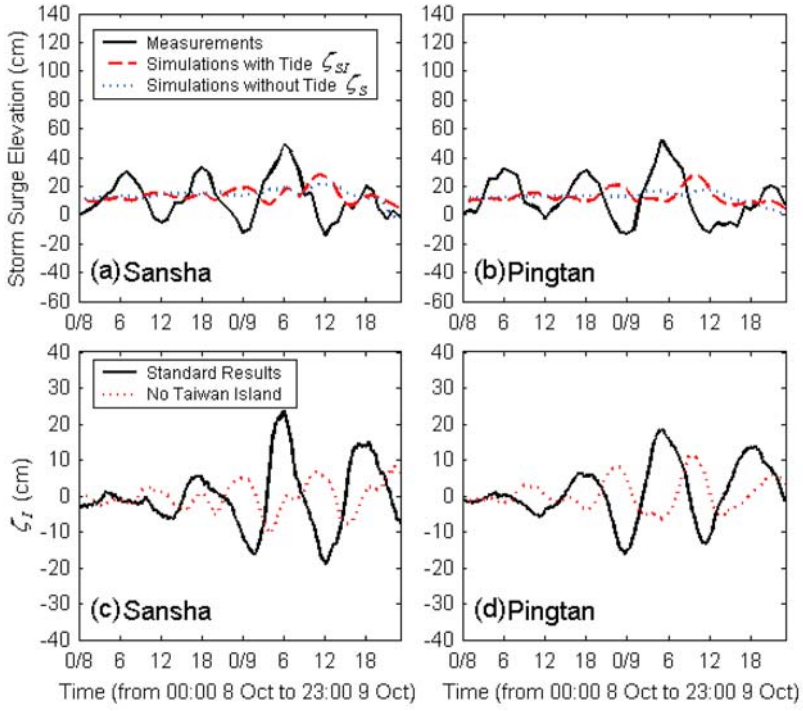

Figure 9. Time series of storm surges, (a and b) measured and simulated in the no-island case and (c and d) simulated residuals due to tide-surge interaction.

model only slightly underpredicted tidal elevation at Sansha and predicted well at Pingtan, indicating that the idealized topography could represent basic topographical features of the Taiwan Strait. The practical surges ζ_{SI} and pure surges ζ_S predicted by the idealized model were compared with measured data at Sansha and Pingtan as shown in Figures 12c and 12d. Comparisons of predicted residuals ζ_I between the standard case and the idealized case are shown in Figures 12e and 12f. The comparisons indicated that the idealized model predicted oscillations in residual ζ_I due to tide-surge interaction similar to those in the standard case except for a smaller amplitude at Sansha and slight phase shift at Pingtan.

5.2.2. Idealized Case Without Island

[37] For the idealized case without island, i.e., case 2, the same comparisons were made as in section 5.2.1 and shown in Figure 13. Comparisons of tidal elevation in Figures 13a and 13b indicated that the idealized model without island underpredicted tidal elevations remarkably at Sansha and Pingtan. Tidal phases predicted by this idealized model are very different from the standard results and harmonically calculated results. Figures 13c–13f show comparisons of oscillations and residuals due to tide-surge interaction. The idealized model without island predicted oscillations much weaker than the idealized model with island.

[38] Since the idealized model without island underpredicted tidal elevations, a possibility to cause this weaker nonlinear interaction could be the underprediction of tide range. In order to check if this is a major reason, we set up another case (named case 3) which is the same as case 2 except tidal input conditions. In case 3, the amplitudes of all tidal constituents were multiplied by a factor to make tidal ranges at Sansha and Pingtan comparable to those in case 1. Figure 14 illustrates the same comparisons as in Figure 13. It is interesting that increasing tidal range did not result in stronger tide-surge interaction. The test confirmed that the weak tide-surge interaction in the case without island was not caused by the underprediction of tidal range.

[39] The results from these cases indicated that small-scale geological features have less influence than the large-scale features on tide propagation and tide-surge interaction in the Taiwan Strait.

5.3. Dynamic Analysis

[40] Two conclusions can be drawn from the numerical experiments above. First, the quadratic bottom friction represents the major nonlinear dynamics in predicting tide-surge interaction in the Taiwan Strait. Second, the large-scale geological feature of the Taiwan Strait plays an important role in the intensification of the nonlinear interaction. It is necessary to find a connection between these two findings.

[41] Since the advective effect and the shallow water effect are not important in tide-surge interaction in the Taiwan Strait, we rewrite the depth-averaged momentum equations (1) and (2) and continuity equation (3) neglecting advective terms and replacing H by h as follows:

$$\frac{\partial u}{\partial t} - fv + \frac{g}{R\cos\varphi}\frac{\partial \zeta}{\partial \lambda} = -\frac{1}{\rho R\cos\varphi}\frac{\partial P_a}{\partial \lambda} + \frac{F_s}{\rho h} - \frac{C_b|\mathbf{q}|u}{h}, \quad (13)$$

$$\frac{\partial v}{\partial t} + fu + \frac{g}{R}\frac{\partial \zeta}{\partial \varphi} = -\frac{1}{\rho R}\frac{\partial P_a}{\partial \varphi} + \frac{G_s}{\rho h} - \frac{C_b|\mathbf{q}|v}{h}, \quad (14)$$

$$\frac{\partial \zeta}{\partial t} + \frac{1}{R\cos\varphi}\left[\frac{\partial (hu)}{\partial \lambda} + \frac{\partial (hv\cos\varphi)}{\partial \varphi}\right] = 0, \quad (15)$$

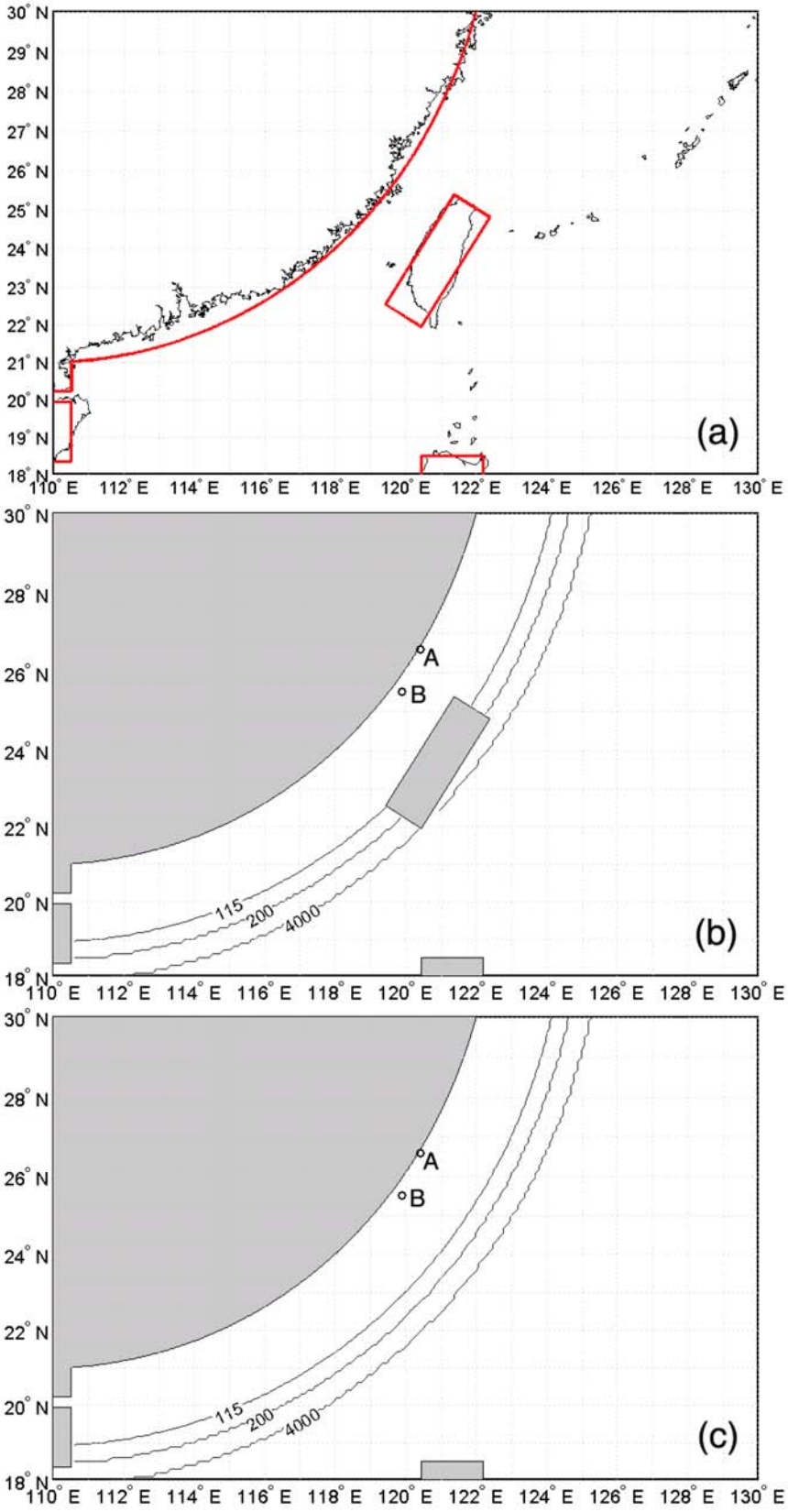

Figure 10. (a) Sketch map of the Taiwan Strait and idealized coastal boundaries, (b) the idealized coastline and bathymetry contours (meters) in the idealized case 1, and (c) the idealized coastline and bathymetry contours (meters) in the idealized cases 2 and 3. Points A and B are locations corresponding to Sansha and Pingtan, respectively.

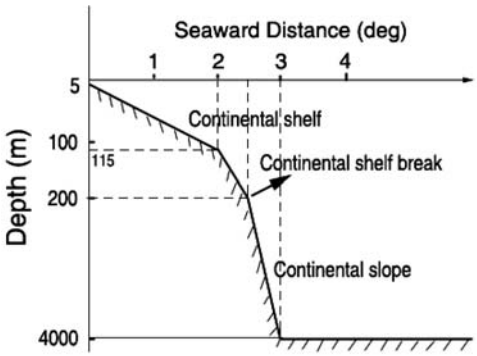

Figure 11. Vertical profile of the idealized bathymetry.

[42] The variables associated with pure tidal motion (u_T, v_T, ζ_T) satisfy equations (13) to (15) with zero-atmosphere forcing, and pure atmosphere-driving motion (u_S, v_S, ζ_S) also satisfy the equations without tidal forcing at open boundaries. Equations for residuals due to tide-surge interaction then follow

$$\frac{\partial u_I}{\partial t} - fv_I + \frac{g}{R\cos\varphi}\frac{\partial \zeta_I}{\partial \lambda} = -\left[\frac{C_b(|\mathbf{q}|u - |\mathbf{q}_T|u_T - |\mathbf{q}_S|u_S)}{h}\right], \quad (16)$$

$$\frac{\partial v_I}{\partial t} + fu_I + \frac{g}{R}\frac{\partial \zeta_I}{\partial \varphi} = -\left[\frac{C_b(|\mathbf{q}|v - |\mathbf{q}_T|v_T - |\mathbf{q}_T|v_S)}{h}\right], \quad (17)$$

$$\frac{\partial \zeta_I}{\partial t} + \frac{1}{R\cos\varphi}\left[\frac{\partial (hu_I)}{\partial \lambda} + \frac{\partial (hv_I\cos\varphi)}{\partial \varphi}\right] = 0, \quad (18)$$

where $u_I = u - u_T - u_S$, $v_I = v - v_T - v_S$ and $\zeta_I = \zeta - \zeta_T - \zeta_S$. Equations (16) and (17) show that the motion associated with the residual is driven by the quadratic friction term. The vector form of the forcing may be written as follows:

$$\boldsymbol{\tau}_I = -\frac{C_b}{h}(|\mathbf{q}|\mathbf{q} - |\mathbf{q}_T|\mathbf{q}_T - |\mathbf{q}_S|\mathbf{q}_S). \quad (19)$$

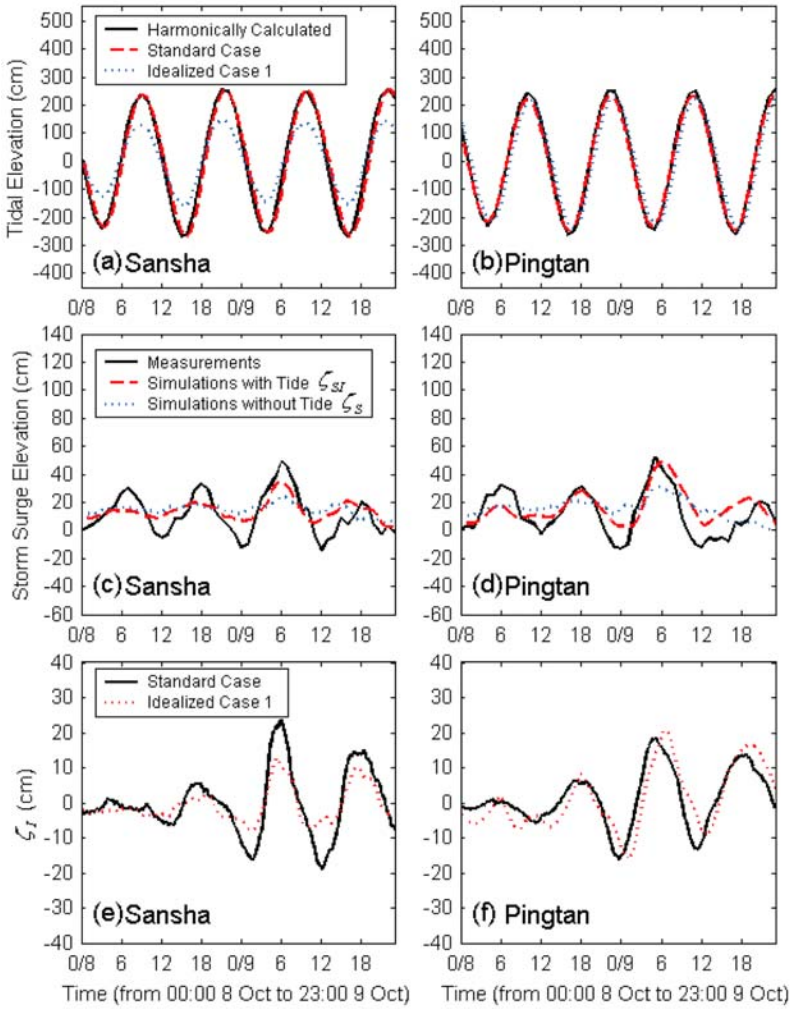

Figure 12. (a and b) Time series of tidal elevations, (c and d) storm surges measured and simulated in the idealized case 1, and (e and f) simulated residuals due to tide-surge interaction.

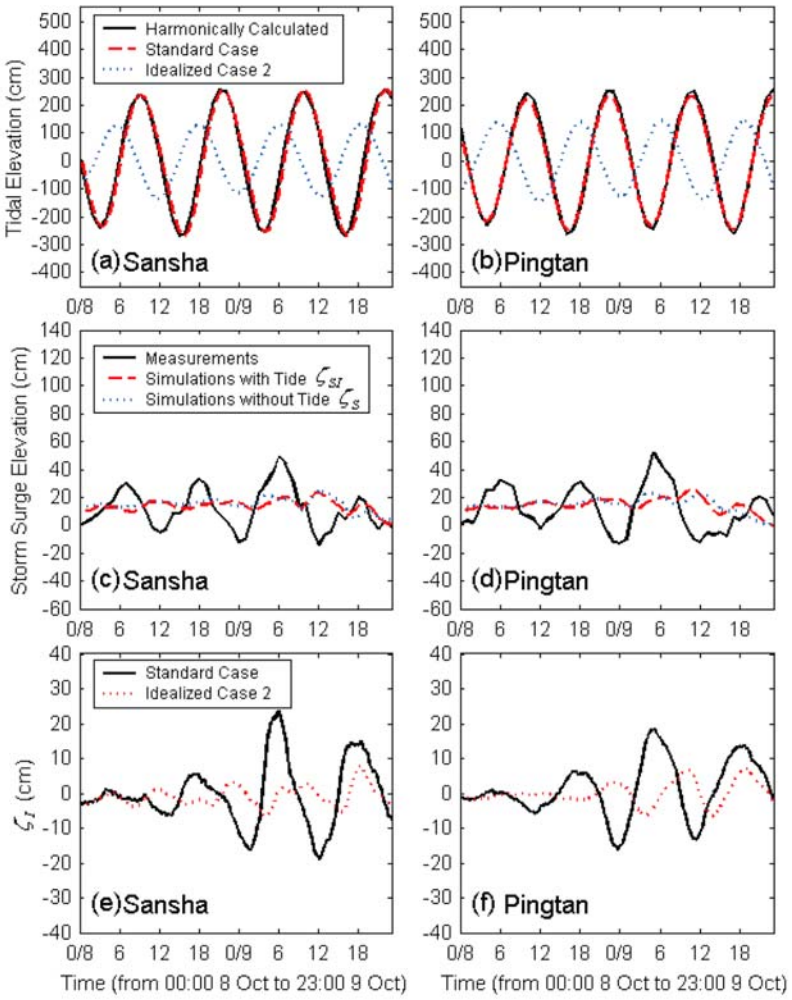

Figure 13. (a and b) Time series of tidal elevations, (c and d) storm surges measured and simulated in the idealized case 2, and (e and f) simulated residuals due to tide-surge interaction.

Replacing $\mathbf{q}$ with $\mathbf{q}_T + \mathbf{q}_S + \mathbf{q}_I$ yields

$$\boldsymbol{\tau}_I = -\frac{C_b}{h}[|\mathbf{q}_T + \mathbf{q}_S + \mathbf{q}_I|(\mathbf{q}_T + \mathbf{q}_S + \mathbf{q}_I) - |\mathbf{q}_T|\mathbf{q}_T - |\mathbf{q}_S|\mathbf{q}_S]. \tag{20}$$

[43] To simplify the discussion, we disregard $\mathbf{q}_I$ in equation (20). The magnitude of the forcing τ_I can be evaluated using the norm of $\boldsymbol{\tau}_I$ which is bounded by (see Appendix A)

$$\frac{2C_b}{h}\left[|\mathbf{q}_T| \cdot |\mathbf{q}_S| - \mathrm{Min}\left(|\mathbf{q}_T|^2, |\mathbf{q}_S|^2\right)\right] \le |\boldsymbol{\tau}_I| \le \frac{2C_b}{h}|\mathbf{q}_T| \cdot |\mathbf{q}_S| \tag{21}$$

[44] The inequality expressed in equation (21) indicates that the magnitude of the forcing $\boldsymbol{\tau}_I$ is dependent on the product of $|\mathbf{q}_T|$ and $|\mathbf{q}_S|$. Increasing $\mathbf{q}_T$ and $\mathbf{q}_S$ may result in increases of the nonlinear interaction. The forcing becomes a maximum when $\mathbf{q}_T$ and $\mathbf{q}_S$ are in the same direction as described in Appendix A.

[45] In the Taiwan Strait, M_2 and K_1 are the major semidiurnal and diurnal tidal constituents, respectively. Both observations and numerical model results have shown that the major axes of their ellipses are in the direction along the strait [*Jan et al.*, 2002; *Lin et al.*, 2005]. Figure 15 shows simulated tidal current ellipses of M_2 and K_1 in the idealized case with island (case 1, top panels) compared with simulations in the case without island (case 2, bottom panels). In the northern portion of the strait, the major axes of both M_2 and K_1 tidal ellipses are basically parallel with the two side banks of the strait in the case with island. In the case without island, the major axes of M_2 are almost normal to the coast. The major axes of K_1 are still parallel with the coast, but magnitudes of its tidal ellipses are rather small compared with those in the case with island. Figure 16 shows snapshots of simulated storm-induced currents during Typhoon Dan in the idealized cases with island (top panels) and without island (bottom panels). In the case with island, storm-induced currents in the northern portion of the strait basically were aligned along the channel direction. In the case without island, storm-induced currents were generally small compared with those in the case with island.

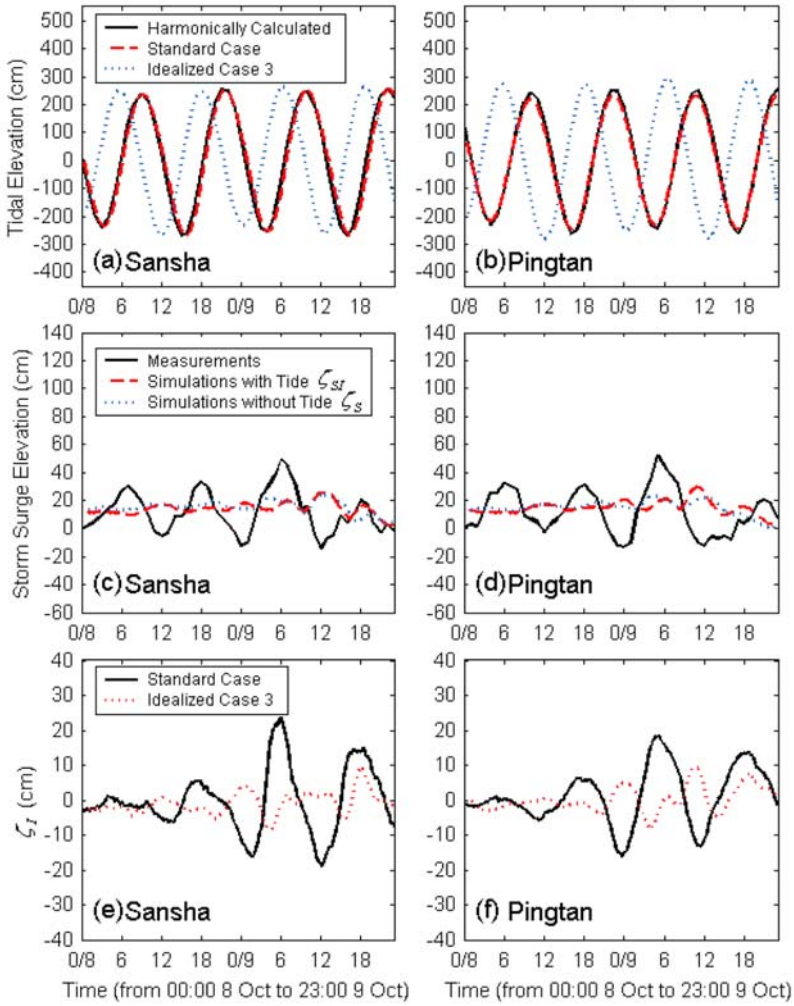

Figure 14. (a and b) Time series of tidal elevations, (c and d) storm surges measured and simulated in the idealized case 3, and (e and f) simulated residuals due to tide-surge interaction.

[46] The simulations above indicate that, with the presence of the island, the channel effect of the strait strengthens both tidal current and storm-induced current and tends to align them along the channel direction in the northern portion of the strait. The force driving tide-surge interaction is thus increased according to the dynamic analysis above. Based on the momentum balance, the increased force of bottom stress is balanced by the pressure gradient force (surface slope) and then the surge residual which indicates the intensity of tide-surge interaction. Therefore, the tide-surge interaction is intensified by the channel effect of the strait. Since the tidal motion is periodic, this process is also periodic and results in the significant oscillations with a tidal period.

6. Conclusion

[47] This study was motivated by obvious oscillations of storm surge elevation with near-tidal period observed along the northern Fujian coast during Typhoon Dan (1999). The results demonstrated that the oscillations were caused by the tide-surge interaction and intensified by the channel effect of the Taiwan Strait. Numerical experiments using reduced models indicated that the nonlinear bottom friction (described by the quadratic bottom friction formula) is the major factor to predict the oscillations due to the tide-surge interaction while the nonlinear advective effect and the shallow water effect have little contribution. Simulations based on simplified topographies with and without the island of Taiwan show that the large-scale geological feature of the strait plays an important role in the intensification of tide-surge interaction. In the presence of the island, the channel effect strengthens both tidal currents and storm-induced currents and trends to align the currents along the channel direction in the northern portion of the Taiwan Strait. Strong tidal currents and storm-induced currents along the channel direction enhance the tide-surge interaction via the nonlinear bottom friction, which results in the obvious oscillations along the northern Fujian coast.

[48] Our model was based on 2-D formulations, and depth-averaged current velocity was used in the bottom stress formulas. Three-dimensional effects on bottom stress, as pointed by *Weisberg and Zheng* [2008], were not taken into

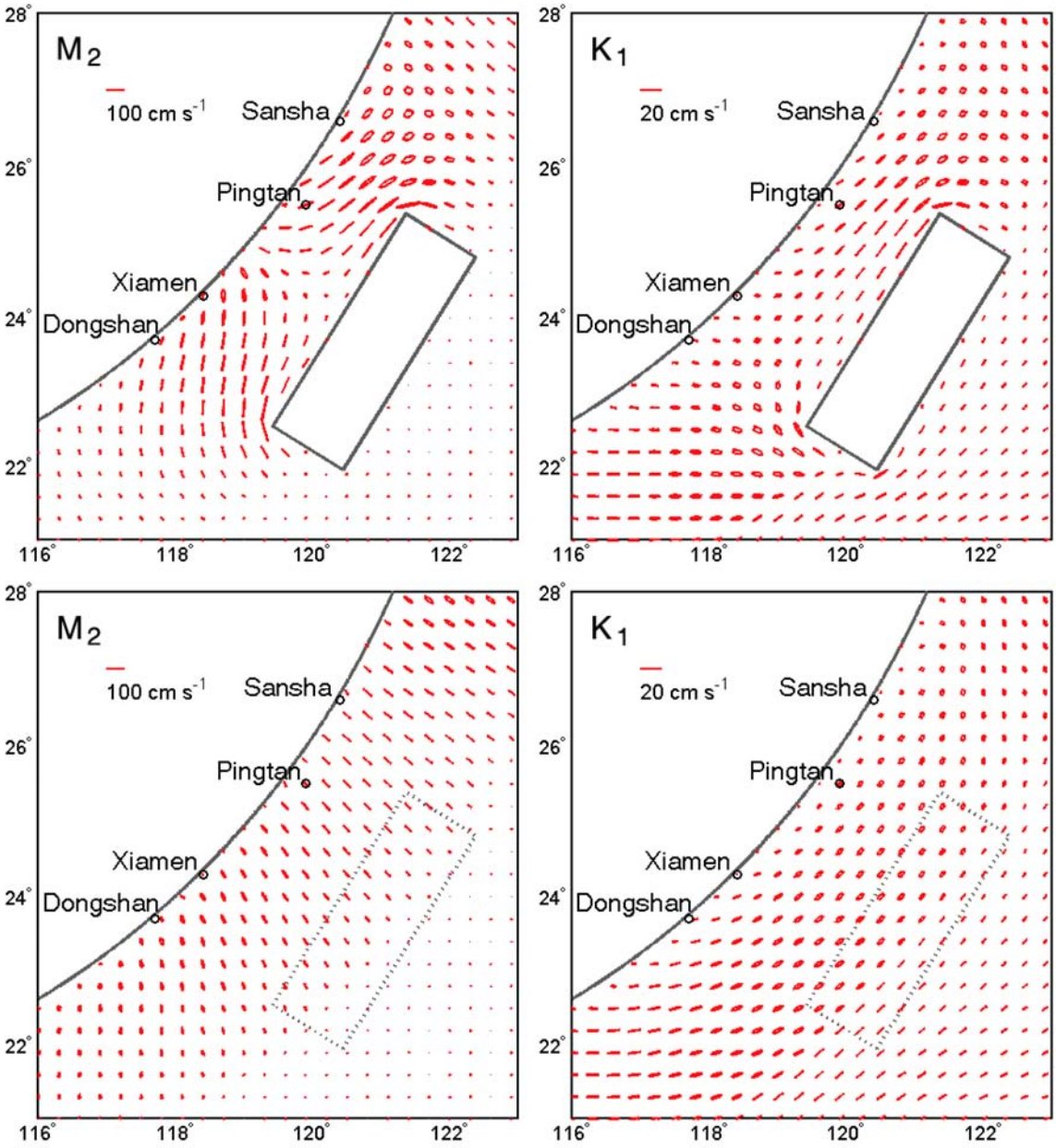

Figure 15. Tidal current ellipses of M_2 and K_1 constituents (top) in the idealized case 1 and (bottom) in the idealized case 2.

account in the present study but may be addressed in the further investigation of tide-surge interaction in the Taiwan Strait.

Appendix A: Derivation of Inequality in Equation (21)

[49] Set

$$\mathbf{q}_T = |\mathbf{q}_T|(\cos\theta_T\mathbf{i} + \sin\theta_T\mathbf{j}) \tag{A1}$$

$$\mathbf{q}_S = |\mathbf{q}_S|(\cos\theta_S\mathbf{i} + \sin\theta_S\mathbf{j}) \tag{A2}$$

where θ_T and θ_S represent velocity angles. Disregarding $\mathbf{q}_I$ in equation (20) we obtained

$$|\tau_I| = \frac{C_b}{h}|(|\mathbf{q}_T + \mathbf{q}_S|)(\mathbf{q}_T + \mathbf{q}_S) - |\mathbf{q}_T|\mathbf{q}_T - |\mathbf{q}_S|\mathbf{q}_S| \tag{A3}$$

$$|\mathbf{q}_T + \mathbf{q}_S| = \left[|\mathbf{q}_T|^2 + |\mathbf{q}_S|^2 + 2|\mathbf{q}_T| \cdot |\mathbf{q}_S|\cos(\theta_T - \theta_S)\right]^{1/2}. \tag{A4}$$

The upper bound value can be obtained when the two velocity vectors are in the same direction, i.e., $\theta_T = \theta_S$:

$$|\tau_I| = \frac{2C_b}{h}|\mathbf{q}_T| \cdot |\mathbf{q}_S| \tag{A5}$$

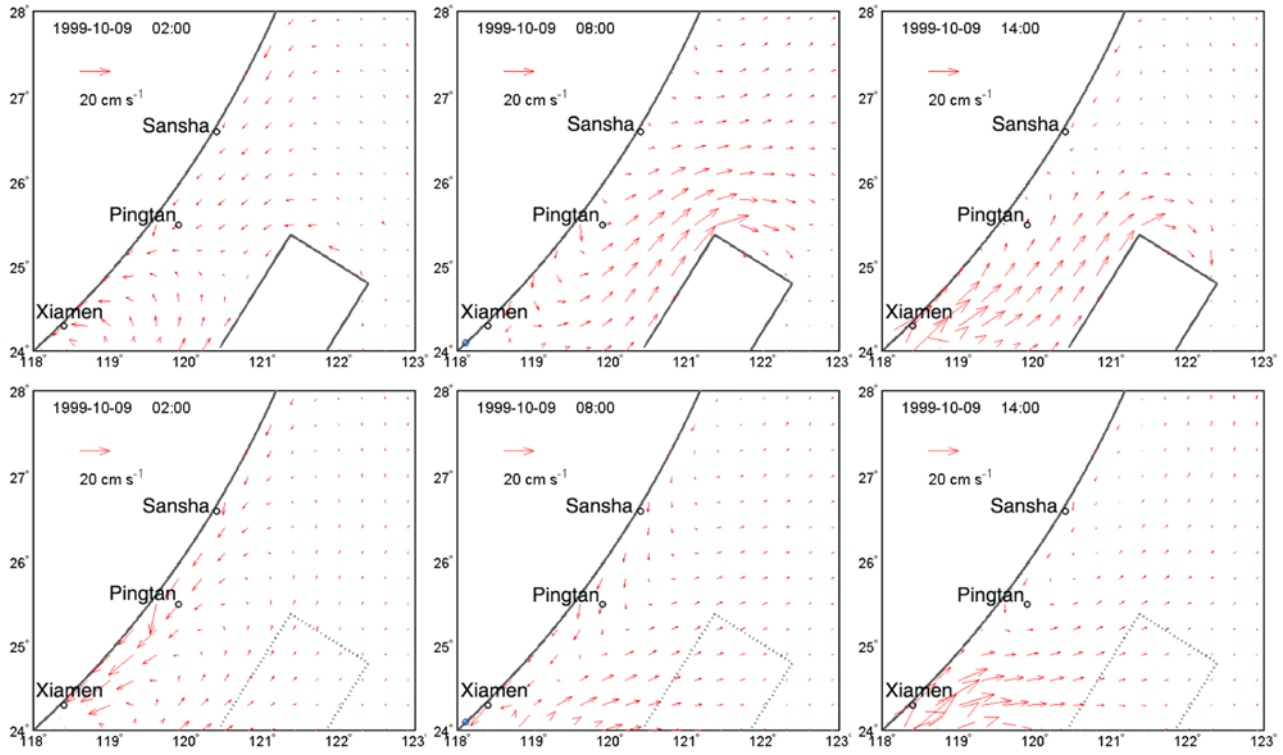

Figure 16. Storm-induced currents caused by Typhoon Dan (1999) (top) in the idealized case 1 and (bottom) in the idealized case 2.

and the lower bound values can be obtained when the two velocity vectors are in the opposite direction, i.e., $\theta_T = \theta_S + \pi$,

$$|\tau_I| = \frac{2C_b}{h}\left[|\mathbf{q}_T| \cdot |\mathbf{q}_S| - \mathrm{Min}\left(|\mathbf{q}_T|^2, |\mathbf{q}_S|^2\right)\right] \qquad \text{(A6)}$$

[50] **Acknowledgments.** This work was jointly supported by the Science Foundation of Fujian Province (2009J01223) and a project of the National High-tech R&D Program (2006AA09A302–6). The first author, W.-Z. Zhang, would like to thank the Center for Applied Coastal Research of University of Delaware for providing research facilities during his post doctoral study. F. Shi and J. T. Kirby would like to acknowledge the support of the National Oceanographic Partnership Program, Project N00014-06-1-0945. Comments from anonymous reviewers were helpful for improving the manuscript.

References

As-Salek, J. A., and T. Yasuda (2001), Tide-surge interaction in the Meghna Estuary: Most severe conditions, *J. Phys. Oceanogr.*, *31*, 3059–3072, doi:10.1175/1520-0485(2001)031<3059:TSIITM>2.0.CO;2.

Atkinson, G. D., and C. R. Holliday (1977), Tropical cyclone minimum sea level pressure/maximum sustained wind relationship for the western North Pacific, *Mon. Weather Rev.*, *105*, 421–427, doi:10.1175/1520-0493(1977)105<0421:TCMSLP>2.0.CO;2.

Banks, J. E. (1974), A mathematical model of a river-shallow sea system used to investigate tide, surge and their interaction in Thames-Southern North Sea region, *Philos. Trans. R. Soc. A*, *275*, 567–609, doi:10.1098/rsta.1974.0002.

Bernier, N. B., and K. R. Thompson (2007), Tide-surge interaction off the east coast of Canada and northeastern United States, *J. Geophys. Res.*, *112*, C06008, doi:10.1029/2006JC003793.

Chang, C. P., T. C. Yeh, and J. M. Chen (1993), Effects of terrain on the surface structure of typhoons over Taiwan, *Mon. Weather Rev.*, *121*, 734–752, doi:10.1175/1520-0493(1993)121<0734:EOTOTS>2.0.CO;2.

Doodson, A. T. (1956), Tides and storm surges in a long uniform gulf, *Proc. R. Soc. Lond. A*, *237*, 325–343, doi:10.1098/rspa.1956.0180.

Fang, G., J. Yang, and X. Zhao (1985), A numerical model for the tides and tidal currents in the Taiwan Strait, *Acta Oceanol. Sin.*, *4*, 189–200.

Feng, S. (1977), A three-dimensional nonlinear model of tides, *Sci. Sin.*, *4*, 436–446.

Flather, R. A. (2000), Existing operational oceanography, *Coastal Eng.*, *41*, 13–40, doi:10.1016/S0378-3839(00)00025-9.

Gray, W. M. (1968), A global view of the origin of tropical disturbances and storms, *Mon. Weather Rev.*, *96*, 669–700, doi:10.1175/1520-0493(1968)096<0669:GVOTOO>2.0.CO;2.

Heaps, N. S. (1969), A two-dimensional numerical sea model, *Philos. Trans. R. Soc. A*, *265*, 93–137, doi:10.1098/rsta.1969.0041.

Holland, G. J. (1980), An analytic model of the wind and pressure profiles in hurricanes, *Mon. Weather Rev.*, *108*, 1212–1218, doi:10.1175/1520-0493(1980)108<1212:AAMOTW>2.0.CO;2.

Horsburgh, K. J., and C. Wilson (2007), Tide-surge interaction and its role in the distribution of surge residuals in the North Sea, *J. Geophys. Res.*, *112*, C08003, doi:10.1029/2006JC004033.

Jakobsen, F., and H. Madsen (2004), Comparison and further development of parametric tropical cyclone models for storm surge modeling, *J. Wind Eng. Ind. Aerodyn.*, *92*, 375–391, doi:10.1016/j.jweia.2004.01.003.

Jan, S., C.-S. Chern, and J. Wang (2002), Transition of tidal waves from the East to South China Seas over the Taiwan Strait: Influence of the abrupt step in the topography, *J. Oceanogr.*, *58*, 837–850, doi:10.1023/A:1022827330693.

Jelesnianski, C. P. (1965), A numerical calculation of storm tides induced by a tropical storm impinging on a continental shelf, *Mon. Weather Rev.*, *93*, 343–358, doi:10.1175/1520-0493(1993)093<0343:ANCOS>2.3.CO;2.

Johns, B., A. D. Rao, S. K. Dube, and P. C. Sinha (1985), Numerical modelling of tide-surge interaction in the bay of Bengal, *Philos. Trans. R. Soc. London, Ser. A*, *313*, 507–535, doi:10.1098/rsta.1985.0002.

Lander, M. A., and C. P. Guard (1998), A look at global tropical cyclone activity during 1995: Contrasting high Atlantic activity with low activity in other basins, *Mon. Weather Rev.*, *126*, 1163–1173, doi:10.1175/1520-0493(1998)126<1163:ALAGTC>2.0.CO;2.

Lin, S. F., T. Y. Tang, S. Jan, and C.-J. Chen (2005), Taiwan strait current in winter, *Cont. Shelf Res.*, *25*, 1023–1042, doi:10.1016/j.csr.2004.12.008.

Liu, F., and X. Wang (1989), A review of storm surge research in China, *Nat. Hazards*, *2*(1), 17–29, doi:10.1007/BF00124755.

Murty, T. S. (1984), Storm surges—meteorological ocean tides, in *Canadian Bulletin of Fisheries and Aquatic Sciences*, 212, 897 pp., Scientific Information and Publications Branch, Ottawa, Canada.

Prandle, D., and J. Wolf (1978), Surge-tide interaction in the South North Sea, in *Nihoul, Hydrodynamics of Estuaries and Fjords (Proceedings of the 9th International Liege Colloquium on Ocean Hydrodynamics)*, edited by J. C. J., pp. 161–185, Amsterdam, Elsevier.

Proudman, J. (1955a), The propagation of tide and surge in an estuary, *Proc. R. Soc. Lond. A*, *231*, 8–24, doi:10.1098/rspa.1955.0153.

Proudman, J. (1955b), The effect of friction on a progressive wave of tide and surge in an estuary, *Proc. R. Soc. Lond. A*, *233*, 407–418, doi:10.1098/rspa.1955.0276.

Proudman, J. (1957), Oscillation of tide and surge in an estuary of finite length, *J. Fluid Mech.*, *2*, 371–382, doi:10.1017/S002211205700018X.

Rossiter, J. R. (1961), Interaction between tide and surge in the Thames, *Geophys. J.*, *6*, 29–53, doi:10.1111/j.1365-246X.1961.tb02960.x.

Shen, J., W. Gong, and H. V. Wang (2006), Water level response to 1999 Hurricane Floyd in the Chesapeake Bay, *Cont. Shelf Res.*, *26*, 2484–2502, doi:10.1016/j.csr.2006.07.021.

Tang, Y. M., R. Grimshaw, B. Sanderson, and G. Holland (1996), A numerical study of storm surges and tides, with application to the North Queensland coast, *J. Phys. Oceanogr.*, *26*, 2700–2711, doi:10.1175/1520-0485(1996)026<2700:ANSOSS>2.0.CO;2.

Wang, J., and F. Chai (1989), Nonlinear interaction between astronomical tides and storm surges at Wusong tidal station, *Chin. J. Oceanology Limnol.*, *7*, 135–142, doi:10.1007/BF02842749.

Wang, X., and F. Liu (1986), The primary study of typhoon surges along Fujian and Guangdong coasts, *Stud. Mar. Sin.*, *27*, 33–43.

Weisberg, R. H., and L. Zheng (2008), Hurricane storm surge simulations comparing three-dimensional with two-dimensional formulations based on an Ivan-like storm over the Tampa Bay, Florida region, *J. Geophys. Res.*, *113*, C12001, doi:10.1029/2008JC005115.

Welander, P. (1961), Numerical prediction of storm surges, *Adv. Geophys.*, *8*, 315–379.

Wolf, J. (1981), Surge-tide interaction in the North Sea and River Thames, in *Floods due to high winds and tides*, edited by D. H. Peregrine, pp. 75–94, Academic, London.

Yang, H., S. Tian, L. Ye, and F. Xu (1993), *Catalog of Marine and Coastal Disasters in China (1949–1990)*, China Ocean Press, Beijing, China.

Zhang, W.-Z., J. Y. Hu, S. P. Shang, M. N. Chen, and W. M. She (2004), On the characteristics of storm surges along Fujian coast, *Mar. Sci. Bull.*, *23*, 12–19.

Zhang, W.-Z., H.-S. Hong, S.-P. Shang, D.-W. Chen, and F. Chai (2007), A two-way nested coupled tide-surge model for the Taiwan Strait, *Cont. Shelf Res.*, *27*, 1548–1567, doi:10.1016/j.csr.2007.01.018.

Zhang, W.-Z., H.-S. Hong, S.-P. Shang, X.-H. Yan, and F. Chai (2009), Strong southward transport events due to typhoons in the Taiwan Strait, *J. Geophys. Res.*, *114*, C11013, doi:10.1029/2009JC005372.

H.-S. Hong and W.-Z. Zhang, State Key Laboratory of Marine Environmental Science, Xiamen University, 422 Siming South Road, Xiamen, Fujian 361005, China. (hshong@xmu.edu.cn)

J. T. Kirby and F. Shi, Center for Applied Coastal Research, Department of Civil and Environmental Engineering, University of Delaware, Newark, DE, USA.

S.-P. Shang, Key Laboratory of Underwater Acoustic Communication and Marine Information Technology of the Minister of Education, Xiamen University, Xiamen, China.